A Method for Measuring the Directional Response of Ultrasound Receivers in the Range 0.3–80 MHz Using a Laser-Generated Ultrasound Source

James A. Guggenheim, Edward Z. Zhang, and Paul C. Beard

***Abstract*— A simple method for measuring the directivity of an ultrasound receiver is described. The method makes use of a custom-designed laser ultrasound source which generates a large diameter (>1 cm) broadband monopolar plane wave with a continuous frequency content extending from ≤330 kHz to ≈80 MHz. The plane wave is highly uniform in amplitude (±5% over >8 mm) and phase (equivalent to <λ/7 at 80 MHz over ≥11 mm). To measure directivity, the source is rotated around the receiver under test in a compact centimeter-scale setup. To demonstrate the method, it was used to measure the directivity of two broadband small aperture Fabry–Perot ultrasound sensors over an angular range of ±50° at frequencies up to 80 MHz. Measurements were found to be highly repeatable with an estimated typical repeatability <4% in the range of 0.5–25 MHz. Due to the broad bandwidth, large size, and adjustable nature of the source, the method is widely applicable and could aid the characterization of receivers used in medical ultrasound, ultrasonic nondestructive testing. and ultrasound metrology.**

***Index Terms*— Broadband, directional sensitivity, directivity, Fabry–Perot (FP), frequency response, laser ultrasound (LUS), ultrasonic variables measurement.**

I. Introduction

THE comprehensive characterization of an ultrasound receiver requires the measurement of its sensitivity, linearity, frequency response, and directivity. The last of these presents several specific challenges in relation to the source requirements. These become particularly demanding when measurements at frequencies in the tens of megahertz range are required, as is the case with the high-frequency transducers increasingly used in high-resolution medical ultrasound [1], photoacoustic imaging [2], industrial nondestructive testing [3], and ultrasound metrology [4].

A critical requirement is that the source emits a large area uniform plane wave. This is necessary to minimize amplitude and phase variations over the receiver surface and reduce errors due to the misalignment between the center of the receiver and the axis of rotation. Measurements may also be required over a wide frequency range extending from the low megahertz to tens of megahertz depending on the bandwidth of the receiver. This necessitates the use of either multiple narrowband sources [5] operating at different frequencies or a single highly broadband source. The former can be time consuming as it requires many measurements, and is prone to alignment errors arising from the substitution of one source for another. A broadband source such as a pulsed transducer can be used to obtain directivity at many frequencies simultaneously [6], [7]. However, it can be challenging to achieve sufficiently broad bandwidth, particularly on a scale of tens of megahertz, using piezoelectric transducers. This is in part due to the resonant nature of piezoelectric ultrasound generation. However, even a heavily damped low Q piezoelectric transducer typically emits a bipolar waveform with a frequency spectrum that rolls off at low frequencies and in this sense is therefore not truly broadband. This limitation can be overcome by exploiting nonlinear propagation [8]. In this approach, the transducer is driven hard at its center frequency to produce a field of high amplitude that propagates nonlinearly. After some propagation distance, the evolution of the field results in a sawtooth wave with a frequency spectrum composed of discretely spaced harmonics. Under these conditions, a field of very broad bandwidth extending from the low megahertz to 100 MHz is achievable. Moreover, because the harmonics decrease as $1/N$, the low frequency components of the field are of high amplitude unlike those of a pulsed bipolar waveform [8], [9]. The disadvantages are that the acoustic field is produced only at integer harmonics of the transducer center frequency (typically 1 MHz). Its spectral content is therefore discontinuous precluding the measurement of directivity as a continuous function of frequency. It also requires a relatively large working distance (≈250 mm [10]) for the field to become fully "shocked" and, in addition, the beamwidth becomes increasingly narrow for increasing harmonics compounding the challenge of achieving accurate alignment and maintaining it during the rotation of the source or receiver.

Another way to generate a highly broadband field is to use a laser-generated ultrasound (LUS) source. This involves irradiating a light-absorbing medium with pulsed laser light leading to the generation of ultrasound via the photoacoustic

Manuscript received July 30, 2017; accepted September 25, 2017. Date of publication September 29, 2017; date of current version December 1, 2017. This work was supported in part by the Engineering and Physical Sciences Research Council and in part by the European Union Project FAMOS under Contract 317744. *(Corresponding author: James A. Guggenheim.)*

The authors are with the Department of Medical Physics and Biomedical Engineering, University College London, London WC1E 6BT, U.K. (e-mail: j.guggenheim@ucl.ac.uk).

Digital Object Identifier 10.1109/TUFFC.2017.2758173

effect [11]. By irradiating a strong light absorber with a laser pulse with a duration of a few nanoseconds in order to ensure near instantaneous energy deposition, it is possible to generate an acoustic field with a bandwidth in the excess of 100 MHz. An LUS source was previously used to measure the directivity of an optical ultrasound sensor [12], but the method suffered from several limitations. First, a point-like source was used, resulting in the generation of a spherical wave. This approach compromises signal-to-noise-ratio (SNR) due to the attenuation arising from the geometric spreading of the wavefront. A spherical wave also provides a poor approximation to a plane wave for all but the smallest receivers and precludes measurements at low frequencies (<10 MHz) owing to its bipolarity. Second, the method required translation of the source with respect to the receiver in order to vary the angle of incidence of the acoustic wave. The acoustic propagation distance (and attenuation) therefore varied as a function of the measurement angle, necessitating a correction that can introduce additional error. A similar approach employing a line source to generate a cylindrical wavefront has been reported [13]. This offers an improvement in SNR due to reduced geometric spreading but is otherwise subject to the above limitations. A different, more promising method used a large (80-mm diameter) planar LUS source to generate a plane wave monopolar acoustic field within which a receiver was rotated [14]. This approach has the advantage that, since the acoustic propagation distance is always constant, there is no requirement to correct for variable attenuation. However, with this first-generation system, the source bandwidth was limited to just 12 MHz (−6 dB), the wavefront exhibited significant heterogeneity with a variation of 6 dB in amplitude and 15% in phase at 10 MHz (equivalent to $\approx\lambda/7$) over ≈30 mm, and the measurement repeatability was not reported. In addition, directivity measurements were made at only six discrete angles in the range of 0°–30°, and the system was not automated but relied on the manual rotation of the receiver and the visual estimation of the angle.

In this paper, a conceptually similar method to that reported in [14], but one with significant refinements and an enhanced performance that has been more comprehensively characterized, is described. It makes use of a different custom-designed planar LUS source to generate a large area, broadband, monopolar plane wave. The source produces a significantly wider bandwidth ranging from very low (≤330 kHz) to very high (approaching 100 MHz) frequencies over a large area (>1 cm diameter). In addition, the wavefront is highly uniform in amplitude (±5% over >8 mm) and phase ($\lambda/7$ at 80 MHz over ≥11 mm). Moreover, by employing a computer controlled, calibrated precision rotation stage, and a carefully designed mechanical assembly for rotating the source, fine angular sampling (<1°) was achieved with high accuracy over a large angular range of +/−50°. These factors along with a fully automated signal acquisition process further enable excellent repeatability to be achieved. As a consequence, the system can perform precise, high-resolution directivity measurements of almost any ultrasound receiver, even those which are relatively large, across a wider frequency range than previously reported.

The remainder of this paper provides a description of the directivity measurement apparatus and procedure followed by a detailed account of the source characterization and system performance. Directivity measurements are then demonstrated for two broadband high-frequency ultrasound receivers and measurement repeatability is estimated.

II. Measurement Apparatus and Procedure

A. Measurement Setup

The apparatus used to measure directivity is shown in Fig. 1(a). The custom-designed LUS source was rotated around the ultrasound receiver under test in a 13 × 19 × 5 cm tank filled with water. The source is shown in detail in Fig. 1(b). It was designed to photoacoustically generate a plane wave through the illumination of a highly absorbing layer deposited on to the outer face of a transparent 8-mm thick, 25-mm diameter polymethylmethacrylate disk fixed at one end of a lens tube. The absorbing layer was a single thin layer of black spray paint (Super Gloss, PlastiKote) which was irradiated through the disk by light delivered through a 1.5-mm diameter multimode optical fiber fixed at the other end of the lens tube. The laser light originated from a 1064-nm Q-switched Nd:YAG laser that emitted 6-ns pulses at a pulse repetition frequency of 20 Hz. The laser beam was attenuated prior to coupling into the fiber by a neutral density (ND) filter that served to limit the energy exiting the fiber to 5-mJ per pulse. Under these conditions, the source generated a monopolar acoustic pulse with a peak pressure of ≈40 kPa at the receiver. By removing the ND filter this could be increased to approximately 0.4 MPa and to higher pressures if needed by reducing the distance between the absorber and fiber tip or using a higher power laser source. The lens tube housing [Fig. 1(b)] is compact, entirely light tight to prevent accidental laser exposure, and the optical fiber is connectorized allowing easy interchangeability between different LUS sources and excitation lasers. In terms of convenience and ease of use therefore, the LUS source compares favourably with conventional piezoelectric sources.

To enable its rotation in precise angular increments, the LUS source was held by a rigid mechanical arm fixed to a motorized rotation stage (PRM1/MZ8, Thorlabs). This was mounted on a manual five-axis (x, y, z, tip, and tilt) positioning system to permit precise alignment.

B. Data Acquisition and Processing

The data acquisition procedure consisted of rotating the source around the receiver in discrete angular steps and acquiring waveforms using a digital storage oscilloscope (DSO; TDS5K, Tektronix) with an analogue bandwidth of 150 MHz. Acquisition was triggered by a photodiode. The time window was set to capture the main acoustic pulse (Section III). The angular range was limited to ±53° by the diameter of the lens tube holding the source [Fig. 1(b)] which makes contact with the inner wall of the water tank at ±54°.

The directivity is given by

$$D_\theta(f) = \frac{|\mathrm{FFT}(s_\theta(t))|}{|\mathrm{FFT}(s_0(t))|} \tag{1}$$

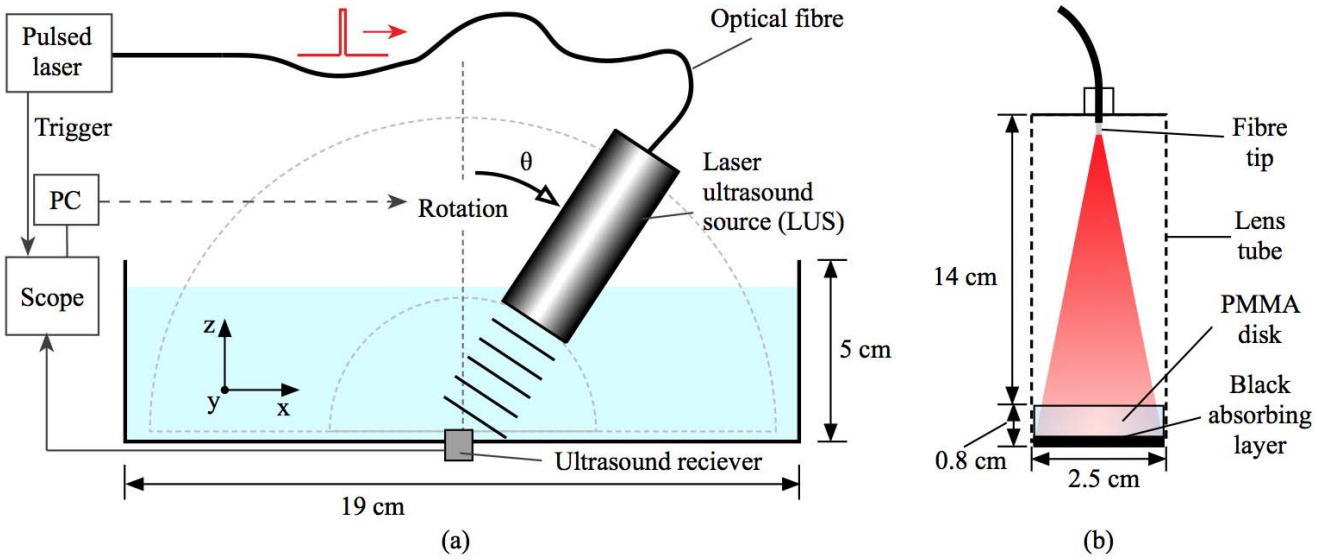

Fig. 1. Directivity measurement apparatus. (a) Complete setup. (b) Cross section through LUS source. PMMA = poly (methyl methacrylate).

where $s_\theta(t)$ is the temporal waveform acquired at angle θ. Prior to computing the fast Fourier transform (FFT), each signal was multiplied by a Tukey window of length 3 μs chosen to minimize spectral leakage without distorting the main pulse and limiting the frequency resolution to 330 kHz.

III. System Characterization

Directivity measurements require a plane wave that is highly uniform in phase, amplitude, and frequency content at least over the dimensions of the active region of the receiver and preferably over a larger area in order to minimize errors arising from misalignment between the receiver and the axis of rotation. Such misalignments produce angle-dependent translation of the wavefront across the receiver which can corrupt the directivity measurement if the wavefront is nonuniform. To examine the structure and frequency content of the field generated by the LUS source, it was mapped using a system based on a broadband Fabry–Perot (FP) polymer film sensor [15], [16]. The FP sensor is an optical ultrasound sensor with a continuously sensitive planar detection surface. Its transduction mechanism [17] is one in which an incident acoustic wave modulates its optical thickness resulting in a corresponding modulation in its optical reflectivity. The acoustic wave can be mapped in 2-D with high resolution by scanning a focused interrogation laser beam point-by-point over the sensor surface using an optical scanner. By virtue of the optical nature of the sensor read-out and transduction mechanism, the system can provide micrometer scale spatial sampling and detection from near dc to frequencies beyond 100 MHz allowing broadband fields to be mapped with high spatiotemporal resolution.

To accurately capture the full range of acoustic frequencies generated by the LUS source, an FP sensor of uniform response from ≈100 kHz to 130 MHz (−3-dB bandwidth) and a cutoff frequency f_c = 200 MHz (where f_c is the frequency at which the sensor response falls to zero) was used. The $1/e^2$ diameter of the interrogation laser beam which, to a first approximation, defines the acoustic element size was 25 μm. The LUS source was positioned at a distance of 35 mm from the sensor and orientated at normal incidence. The interrogation laser beam was scanned in 50-μm steps along an 11-mm line on the sensor and an acoustic waveform was acquired at each step. The waveforms recorded over the entire line scan were mapped to a linear gray scale and displayed as a 2-D image, as shown in Fig. 2(a). This image shows the primary plane wave (P) emitted by the source followed by the arrival of lower amplitude edge waves (E) originating from its perimeter. Fig. 2(b) shows the waveform acquired at $x = 0$ with the edge waves time-gated out to show just the primary wave (P). The primary pulse is evidently near-monopolar with minimal distortion and ringing. The FFT of this signal was calculated following its multiplication by a Tukey window of length 3 μs. The resultant frequency spectrum is plotted in Fig. 2(c). It exhibits a smooth roll-off from ≤330 kHz, limited by the window length, to ≈80 MHz, limited by acoustic attenuation in the coupling medium (water). Fig. 2(c) shows that, unlike the characteristic bipolar waveform produced by a conventional piezoelectric source, the near-monopolar nature of the wave results in minimal roll-off at low frequencies. Note that at 40 kPa (the peak pressure of the acoustic field), even at 80 MHz the shock formation distance is greater than the source–receiver distance. Hence nonlinear effects are likely to be modest and have minimal impact on the measurement.

The phase uniformity of the plane wave (P) illustrated in Fig. 2(a) was assessed by measuring its time of arrival (TOA) as a function of position. The time point at which each waveform in the line scan first exceeded 50% of its peak value was identified yielding the TOA to within ±2 ns, limited by the temporal sampling interval of the DSO. A straight line was then fit to these values over the entire 11-mm line scan.

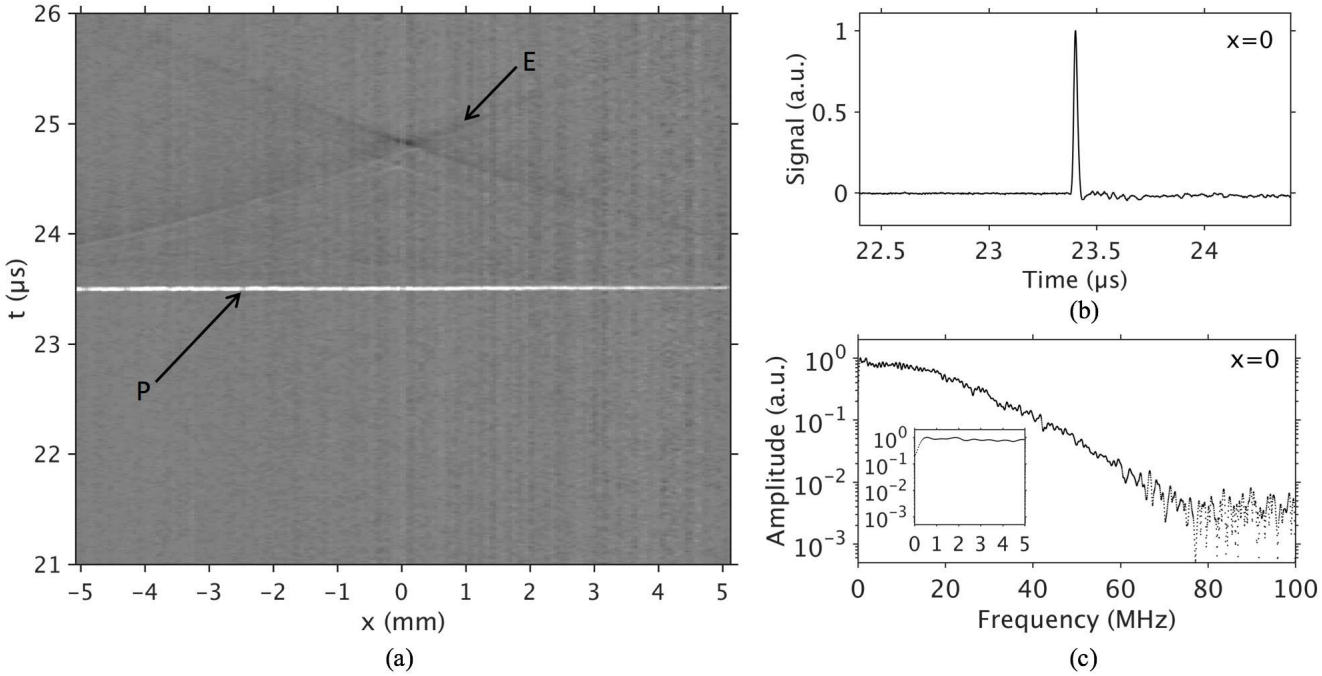

Fig. 2. LUS field characterization. (a) Ultrasound field generated by the LUS source mapped by an FP sensor with a 130-MHz −3-dB bandwidth. Step size = 50 μm and temporal sampling interval = 4 ns. P: initial plane wave and E: edge wave component. (b) Waveform (at $x = 0$) time gated to select only the initial plane wave P. The signal was averaged over 1000 acquisitions. (c) FFT of the waveform in (b) following the application of a Tukey window of length 3 μs centered on the main pulse. Inset: expanded view of frequency spectrum between 0 and 5 MHz.

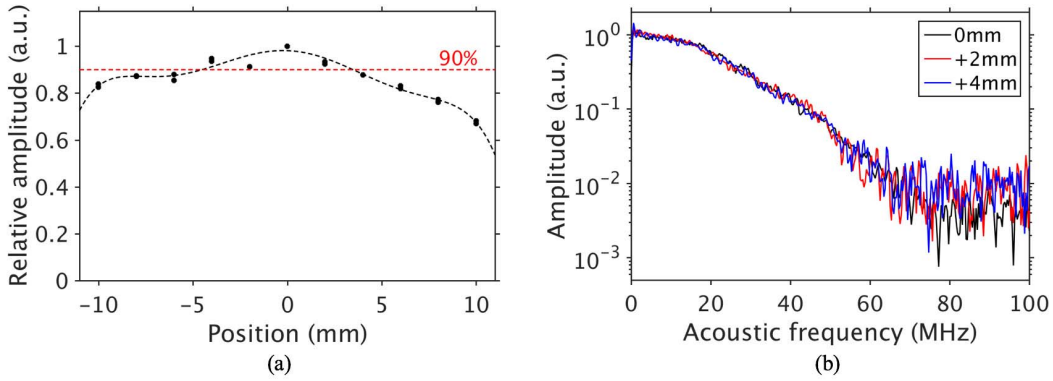

Fig. 3. LUS field uniformity. (a) Peak (normal incidence) amplitude of the ultrasonic pulse as a function of laterally translated source position. (b) FFT of signals acquired at lateral translations of 0, 2, and 4 mm [from the center of the scan in (a)].

For each waveform the difference between the TOA and the corresponding point on the straight line was recorded. The mean absolute difference from the straight line was 1.8 ns. This indicates a flatness of ± 2.7 μm; equivalent to $\lambda/7$ at 80 MHz, which shows that the phase variation across the wavefront is small over the full extent of the source bandwidth.

The amplitude uniformity along the wavefront was assessed by operating the FP sensor at a single fixed point and translating the source laterally in steps of 2 mm over a total distance of 22 mm. The reason for mapping the field amplitude in this way (as opposed to keeping the source in a fixed position and scanning the interrogation laser beam over the surface of the FP sensor as above) was to avoid errors due to spatial variations in the FP sensor sensitivity. Fig. 3(a) shows the relative peak amplitude measured at each position. Although the maximum variation in amplitude was ≈30% over the full 22-mm scan, the amplitude was constant to within ±5% over a distance of at least 8 mm. The variations in amplitude are likely to be due to the nonuniform spatial profile of the incident illumination beam arising from the multimode nature of the light propagation within the optical fiber and imperfections in the absorbing layer. FFTs of the signals acquired at lateral translations of 0, 2, and 4 mm are shown in Fig. 3(b). The frequency spectra appear to be highly consistent showing that the source retains its full bandwidth over a substantial distance; at least 4 mm in one direction suggesting, due to the circular symmetry of the source, a uniform area ≥8 mm in diameter. Overall, these results suggest that the source emits a plane wave that exhibits excellent uniformity in terms of amplitude, phase, and frequency content over a centimeter length scale.

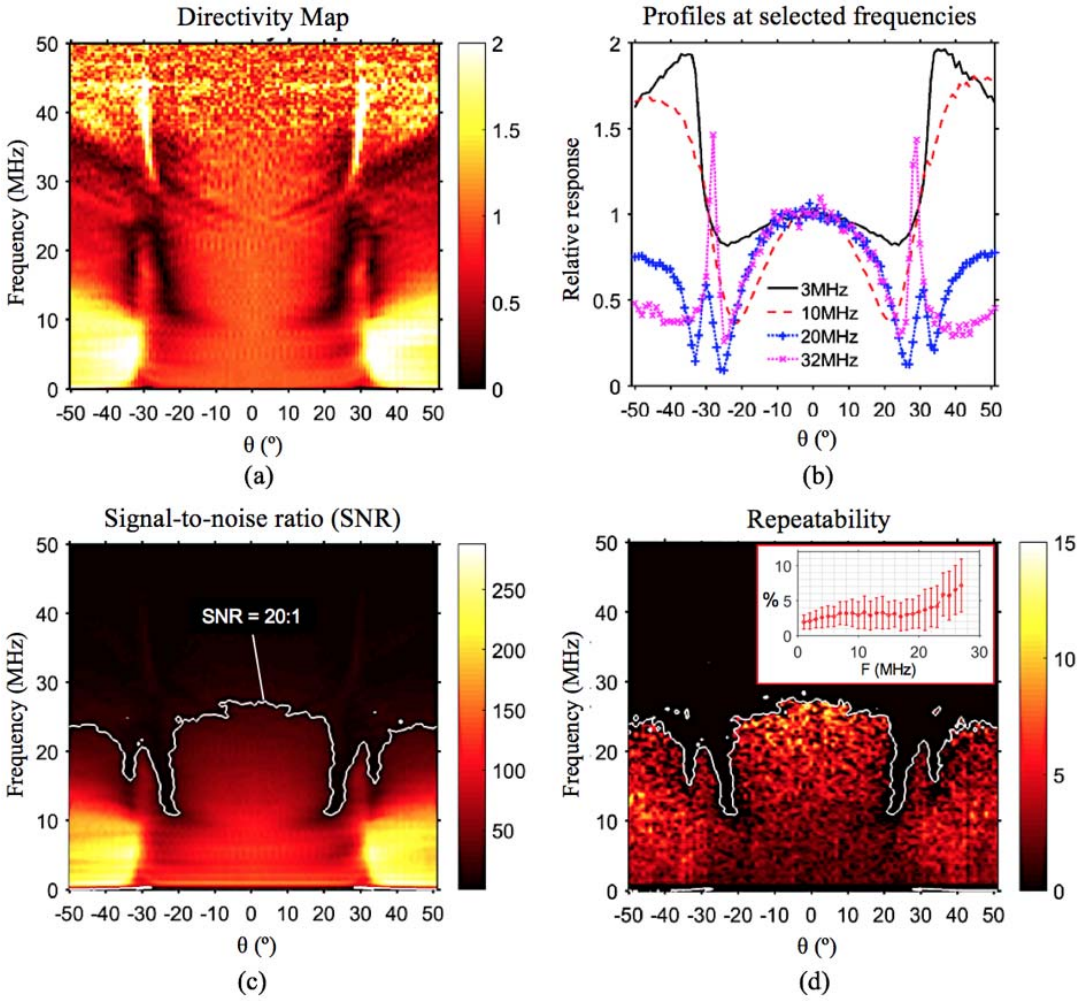

Fig. 4. Directivity of an FP ultrasound sensor with a 16-MHz −3-dB bandwidth obtained over five repeats with 20 signal averages per angle, an angular range of $-50° \leq \theta \leq 51°$, and an angular step size of 1°. (a) Mean 2-D directivity map. (b) Directivity at selected frequencies (profiles through the map). (c) Mean estimated SNR (contour line shows the cutoff at which SNR = 20:1). (d) Estimated repeatability at each frequency and angle (in the region of SNR > 20:1). Inset: mean repeatability value as a function of frequency, error bars show 1 standard deviation.

IV. Directivity Measurements

A. Example Measurement and Repeatability Estimate

To demonstrate the system, the directivity of an FP sensor with a 16-MHz −3-dB bandwidth and $f_c = 44$ MHz was measured. These sensors are typically challenging to assess due to their small element size and large bandwidth. The sensor was constructed as described previously [16]. It had dielectric mirror coatings and a 50-μm-thick parylene C spacer. The interrogation laser beam diameter ($2\omega_0$) was 25 μm. To obtain an indication of repeatability, the measurement was repeated five times.

The directivity was calculated from the measured data using (1) and averaged across all five data sets. The results were mapped to a linear color scale and plotted as a 2-D directivity map, as shown in Fig. 4(a). The directivity at selected frequencies was obtained by taking horizontal profiles through this map, as illustrated in Fig. 4(b). The map and profiles show a region of relatively uniform response near to normal incidence with a smooth roll-off to first minima at approximately ±25° and second minima at 33°. The latter are critical angle effects as described in [6]. At these angles, the ultrasonic wavefronts are propagating almost horizontally within the sensor so there is negligible displacement in the vertical direction and the sensor response falls to zero. The map is symmetric and shows the response up to ≈35 MHz. Beyond this frequency, noise dominates due to reduced SNR, a consequence of the roll-off in the source spectrum and sensor response as well as the increased acoustic attenuation in the acoustic coupling fluid (water) at higher frequencies.

To obtain a meaningful estimate of repeatability that is representative of the measurement method, rather than the characteristics of the specific receiver under test, the repeatability was assessed only in those regions of the response map that exhibited high SNR. The SNR was estimated by comparing the power spectrum of each angularly resolved waveform to that of just the data recorded prior to the arrival of the acoustic pulse (noise only). The SNR estimate is plotted in Fig. 4(c) with a contour line at SNR = 20:1. Repeatability was then computed only in the region of SNR > 20:1. The repeatability was computed as the standard deviations of the values in the directivity maps obtained over five repeats and plotted as percentages of the normal incidence response. The repeatability map still shows some variations due to noise and

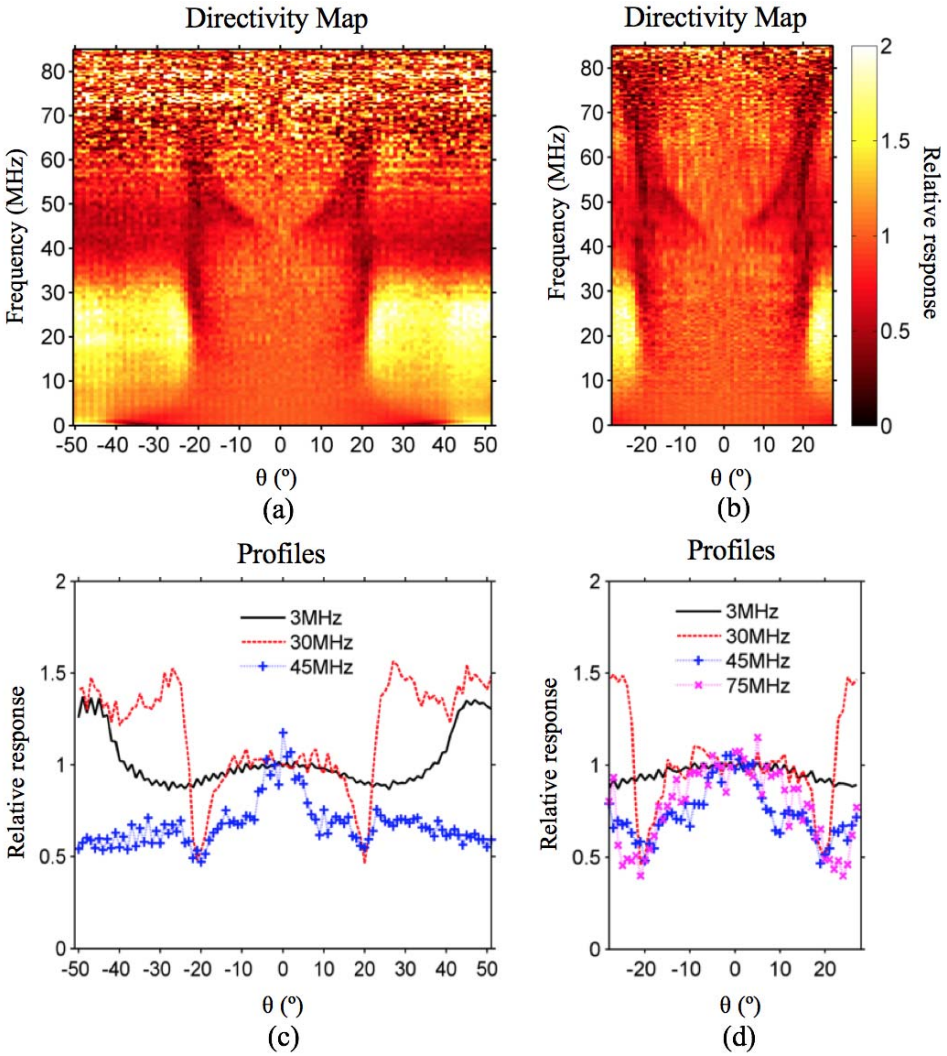

Fig. 5. Directivity of an FP ultrasound sensor with an 80-MHz −3-dB bandwidth obtained with 200 signal averages per angle, two different angular ranges, and an angular step of 1°. (a) Directivity map obtained with an angular range of $-50° \leq \theta \leq 51°$. (b) Directivity map obtained with a reduced working distance and reduced angular range of $-27° \leq \theta \leq 27°$. (c) and (d) Profiles through each response map.

a tendency for repeatability to decrease at higher frequencies and angles, where the effect of errors due to misalignment and wavefront nonuniformities is more pronounced. The mean and standard deviation of the repeatability were calculated as a function of frequency and plotted in the inset of Fig. 4(d). The mean repeatability increases with frequency over the studied range from ≈2% at 1 MHz to ≈7% at 27 MHz. The system is therefore highly repeatable even up to relatively high (10 s of megahertz) frequencies.

B. Example Measurement With High-Frequency and High-Resolution Data

The maximum frequency of the directivity measurement (≈35 MHz) in the previous section was primarily limited by the bandwidth of the sensor under test. In order to demonstrate the system over a larger bandwidth, the 16-MHz sensor was replaced with one that had an estimated −3-dB bandwidth of 80 MHz and $f_c \approx 180$ MHz. This sensor had mirror coatings composed of different materials and a thinner 12-μm-thick parylene C spacer, and was therefore expected to have a different directional response. The resultant response map and directivity profiles are shown in Fig. 5(a) and (c). The map shows the response up to ≈65 MHz, beyond which noise dominates. Compared to the 16-MHz sensor (Fig. 4), the response is clearly different due to differences in the structure and material properties of the two sensors. However, there are some common features such as a region of relatively uniform response near to normal incidence with a roll-off to symmetric minima at, in this case, ±20° due to critical angle effects.

To demonstrate the ability of the system to measure at even higher frequencies, this measurement was repeated with a reduced working distance so as to reduce the acoustic attenuation by the coupling medium (water). This also had the effect of reducing the available angular range. The results are displayed in Fig. 5(b) and (d). As expected, these are highly consistent with those of the previous measurement up to 65 MHz beyond which additional features are now discernible. For example, the profile at 75 MHz [Fig. 5(d)]

shows symmetric minima at ($\pm$) $\approx$22° and the directivity map [Fig. 5(b)] clearly shows the response up to $\approx$80 MHz.

V. Conclusion

A simple, practical, and versatile experimental arrangement for measuring the directivity of ultrasound receivers using a custom-designed plane wave LUS source has been developed. Through the pulsed illumination of a planar absorbing layer, the source generates a large area (>1 cm diameter) monopolar plane wave with a broad continuous bandwidth to 80 MHz and excellent amplitude and phase uniformity. The method provides high repeatability (<7% for frequencies up to 27 MHz). It also allows near arbitrary adjustment of the source diameter by varying the beam diameter. All of this represents a level of acoustic performance and versatility that would be difficult, if not impossible, to achieve using conventional piezoelectric sources. Moreover, since the measurements are made in the near field, a relatively short (<4 cm) fixed working distance is used allowing for a compact and convenient benchtop setup. The system was demonstrated by successfully making high-resolution directivity measurements of two planar FP ultrasound sensors, which are typically challenging to assess due to their small element size and large bandwidth. While the system has been used in this paper to acquire maps of the relative magnitude directional response, it is also possible in principle to extract the relative phase response from the same data.

In its current form, the system provides sufficient bandwidth and wavefront uniformity to characterize the majority of ultrasound receivers used in medical and industrial ultrasound which typically operate at frequencies below 100 MHz with elements of sub-centimeter dimensions. However, there remains scope to adjust the source characteristics to assess higher frequency or larger aperture receivers if required. The current method is limited to a maximum frequency of 80 MHz due to the finite bandwidth of the source and acoustic attenuation in the coupling medium. However, it is estimated that the source bandwidth could be extended to at least 200 MHz by using shorter laser pulses, reducing the thickness of the absorbing coating and decreasing the acoustic propagation distance [12]. For characterizing very large area receivers of centimeter scale dimensions, the source diameter could readily be increased by increasing the beam diameter. This may also require improving the amplitude uniformity which could be achieved by the use of beam shaping optics and diffusing elements in order to produce a top-hat spatially smooth beam profile.

In summary, the method described in this paper enables the directivity of ultrasound receivers to be measured easily and repeatably over a large bandwidth. It therefore represents a useful characterization tool, particularly for measuring the directivity of broadband high-frequency receivers used in medical and industrial ultrasound.

Acknowledgment

The authors would like to thank Dr. A. Hurrell from Precision Acoustics, Dorset, U.K., and Dr. E. Martin and Dr. B. Cox from UCL, London, U.K., for their useful discussions. They would also like to thank J. Evans from UCL for his technical support.

References

[1] K. K. Shung, "High frequency ultrasonic imaging," *J. Med. Ultrasound*, vol. 17, no. 1, pp. 25–30, Jan. 2009.
[2] P. Beard, "Biomedical photoacoustic imaging," *Interface Focus*, vol. 1, no. 4, pp. 602–631, Jun. 2011.
[3] B. W. Drinkwater and P. D. Wilcox, "Ultrasonic arrays for non-destructive evaluation: A review," *NDT E Int.*, vol. 39, no. 7, pp. 525–541, Oct. 2006.
[4] S. Umchid *et al.*, "Development of calibration techniques for ultrasonic hydrophone probes in the frequency range from 1 to 100 MHz," *Ultrasonics*, vol. 49, no. 3, pp. 306–311, Mar. 2009.
[5] D. G. Shombert, S. W. Smith, and G. R. Harris, "Angular response of miniature ultrasonic hydrophones," *Med. Phys.*, vol. 9, no. 4, p. 484, 1982.
[6] B. T. Cox and P. C. Beard, "The frequency-dependent directivity of a planar Fabry-Pérot polymer film ultrasound sensor," *IEEE Trans. Ultrason., Ferroelect., Freq. Control*, vol. 54, no. 2, pp. 394–404, Feb. 2007.
[7] G. R. Harris and D. G. Shombert, "A pulsed near-field technique for measuring the directional characteristics of acoustic receivers," *IEEE Trans. Sonics Ultrason.*, vol. SU-32, no. 6, pp. 802–808, Jun. 1985.
[8] R. A. Smith and D. R. Bacon, "A multiple-frequency hydrophone calibration technique," *J. Acoust. Soc. Amer.*, vol. 87, no. 5, pp. 2231–2243, May 1990.
[9] P. C. Beard, A. M. Hurrell, and T. N. Mills, "Characterization of a polymer film optical fiber hydrophone for use in the range 1 to 20 MHz: A comparison with PVDF needle and membrane hydrophones," *IEEE Trans. Ultrason., Ferroelect., Freq. Control*, vol. 47, no. 1, pp. 256–264, Jan. 2000.
[10] A. Hurrell, private communication, Mar. 2017.
[11] S. J. Davies, C. Edward, G. S. Taylor, and S. B. Palmers, "Laser-generated ultrasound: Its properties, mechanisms and multifarious applications," *J. Phys. D, Appl. Phys.*, vol. 26, no. 3, pp. 329–348, 1993.
[12] H. Li, B. Dong, Z. Zhang, H. F. Zhang, and C. Sun, "A transparent broadband ultrasonic detector based on an optical micro-ring resonator for photoacoustic microscopy," *Sci. Rep.*, vol. 4, p. 4496, Jan. 2014.
[13] J. Rebling, O. Warshavski, C. Meynier, and D. Razansky, "Broadband optoacoustic characterization of cMUT and PZT transducer directivity in receive mode," *Proc. SPIE*, vol. 10139, p. 101391K, Mar. 2017.
[14] A. Conjusteau, S. A. Ermilov, R. Su, H.-P. Brecht, M. P. Fronheiser, and A. A. Oraevsky, "Measurement of the spectral directivity of optoacoustic and ultrasonic transducers with a laser ultrasonic source," *Rev. Sci. Instrum.*, vol. 80, no. 9, p. 093708, 2009.
[15] E. Zhang and P. Beard, "Broadband ultrasound field mapping system using a wavelength tuned, optically scanned focused laser beam to address a Fabry Pérot polymer film sensor," *IEEE Trans. Ultrason., Ferroelect., Freq. Control*, vol. 53, no. 7, pp. 1330–1338, Jul. 2006.
[16] E. Zhang, J. Laufer, and P. Beard, "Backward-mode multiwavelength photoacoustic scanner using a planar Fabry–Perot polymer film ultrasound sensor for high-resolution three-dimensional imaging of biological tissues," *Appl. Opt.*, vol. 47, no. 4, pp. 561–577, Mar. 2008.
[17] P. C. Beard, F. Perennes, and T. N. Mills, "Transduction mechanisms of the Fabry-Perot polymer film sensing concept for wideband ultrasound detection," *IEEE Trans. Ultrason., Ferroelect., Freq. Control*, vol. 46, no. 6, pp. 1575–1582, Nov. 1999.

James A. Guggenheim, photograph and biography not available at the time of publication.

Edward Z. Zhang, photograph and biography not available at the time of publication.

Paul C. Beard, photograph and biography not available at the time of publication.